The Astrophysical Journal, 977:211 (9pp), 2024 December 20 https://doi.org/10.3847/1538-4357/ad8b9c

Do Neutron Star Ultraluminous X-Ray Sources Masquerade as Intermediate-mass Black Holes in Radio and X-Ray?

Teresa Panurach[1], Kristen C. Dage[2,3], Ryan Urquhart[4], Richard M. Plotkin[5,6], Jeremiah D. Paul[5], Arash Bahramian[3], McKinley C. Brumback[7], Timothy J. Galvin[8], Isabella Molina[4], James C. A. Miller-Jones[3], and Payaswini Saikia[9]
[1] Center for Materials Research, Department of Physics, Norfolk State University, Norfolk, VA 23504, USA; tpanurach@nsu.edu
[2] Department of Physics and Astronomy, Wayne State University, 666 W Hancock St, Detroit, MI 48201, USA
[3] International Centre for Radio Astronomy Research—Curtin University, GPO Box U1987, Perth, WA 6845, Australia
[4] Center for Data Intensive and Time Domain Astronomy, Department of Physics and Astronomy, Michigan State University, East Lansing, MI 48824, USA
[5] Department of Physics, University of Nevada, Reno, NV 89557, USA
[6] Nevada Center for Astrophysics, University of Nevada, Las Vegas, NV 89154, USA
[7] Department of Physics, Middlebury College, Middlebury, VT 05753, USA
[8] CSIRO Space & Astronomy, PO Box 1130, Bentley, WA 6102, Australia
[9] Center for Astro, Particle and Planetary Physics, New York University Abu Dhabi, PO Box 129188, Abu Dhabi, UAE
Received 2024 June 17; revised 2024 October 11; accepted 2024 October 12; published 2024 December 13

Abstract

Ultraluminous X-ray sources (ULXs) were once largely believed to be powered by super-Eddington accretion onto stellar-mass black holes, although in some rare cases, ULXs also serve as potential candidates for (sub-Eddington) intermediate-mass black holes. However, a total of eight ULXs have now been confirmed to be powered by neutron stars, thanks to observed pulsations, and may act as contaminants for the radio/X-ray selection of intermediate-mass black holes. Here, we present the first comprehensive radio study of seven known neutron star ULXs using new and archival data from the Karl G. Jansky Very Large Array and the Australia Telescope Compact Array, combined with the literature. Across this sample, there is only one confident radio detection, from the Galactic neutron star ULX Swift J0243.6+6124. The other six objects in our sample are extragalactic, and only one has coincident radio emission, which we conclude is most likely contamination from a background H II region. We conclude that with current facilities, neutron star ULXs do not produce significant enough radio emission to cause them to be misidentified as radio-/X-ray-selected intermediate-mass black hole candidates. Thus, if background star formation has been properly considered, the current study indicates that a ULX with a compact radio counterpart is not likely to be a neutron star.

Unified Astronomy Thesaurus concepts: Neutron stars (1108); Compact objects (288); Ultraluminous x-ray sources (2164)

1. Introduction

Ultraluminous X-ray sources (ULXs) are bright, off-nuclear binary systems and primarily extragalactic. These systems are known to host compact objects, and their observed X-ray luminosities (L_x) exceed the Eddington limit (L_{Edd}) for a $10M_\odot$ black hole, $L_x \sim 10^{39}$ erg s^{-1}. Because of their high luminosities, the population of ULXs was thought to be powered entirely by black holes, and some ULXs were also initially put forward as the missing class of intermediate-mass black holes (IMBHs; G. Fabbiano 1989). However, the discovery of pulsations from ULX M82 X-2 (M. Bachetti et al. 2014) disrupted the traditional ULX paradigm and presented just the first of many super-Eddington neutron star ULX discoveries. It is now often suggested that most, if not all, ULXs may be powered by neutron stars (e.g., D. J. Walton et al. 2018; A. King & J.-P. Lasota 2019; see also the reviews from P. Kaaret et al. 2017; S. N. Fabrika et al. 2021; A. King et al. 2023; K. C. Dage & K. Kovlakas 2024).

While pulsations are the best way to secure the identification of a neutron star primary, pulsations in ULXs are transient (M. Bachetti et al. 2014; F. Furst et al. 2016; G. L. Israel et al. 2017d; S. Carpano et al. 2018). Because of a number of factors, such as geometry, thick outflows, and disk warps, it is difficult to properly distinguish between potential black hole ULXs and neutron star ULXs. That is, if pulsations are not observed, the object could still be a neutron star, with the site of pulsations obscured. As of yet, especially from X-rays alone, there is no metric to identify black hole ULXs and hence quantify if black holes represent a significant portion of the population of ULXs.

At low accretion rates, it has previously been suggested that the ratio of radio to X-ray luminosity can distinguish black hole candidates from other classes of accreting compact objects (T. J. Maccarone 2005), both in the stellar- ($\approx 10M_\odot$; e.g., J. Strader et al. 2012; L. Chomiuk et al. 2013; J. C. A. Miller-Jones et al. 2015; L. Shishkovsky et al. 2018; Y. Zhao et al. 2020; V. Tudor et al. 2022) and intermediate-mass ranges ($\approx 10^3$–$10^5 M_\odot$; e.g., K. Nyland et al. 2012; N. Webb et al. 2012; R. S. Barrows et al. 2019; A. E. Reines et al. 2020; A. Paduano et al. 2024). The reason stems from black hole X-ray binaries (XRBs) in the hard-X-ray spectral state displaying compact radio emission (R. P. Fender 2001; S. Corbel & R. P. Fender 2002), which arises from a partially self-absorbed synchrotron jet (R. D. Blandford & A. Königl 1979). In the hard state (when $L_X \lesssim 0.01 L_{Edd}$), where black hole XRBs begin and end outbursts, they display a nonlinear correlation between their radio (L_R) and X-ray luminosities (which we will refer to as the radio/X-ray luminosity correlation; E. Gallo et al. 2003; S. Corbel et al. 2003). While there is some overlap in the ratios of radio to X-ray luminosities (L_R/L_X) between black hole and

neutron star XRBs, at a given L_X, black hole XRBs tend to have larger L_R/L_X ratios by a factor of ≈20 on average (E. Gallo et al. 2018). Additionally, A. Merloni et al. (2003) and H. Falcke et al. (2004) demonstrated that by including a mass-normalization term, the radio/X-ray luminosity correlation can be extended to supermassive ($>10^6\,M_\odot$) analogs of hard-state black hole XRBs, through a nonlinear correlation among L_R, L_X, and the black hole mass M_{BH}, which is termed the fundamental plane of black hole activity. Similar work has been done for neutron stars (e.g., E. Gallo et al. 2018; N. V. Gusinskaia et al. 2020; T. Panurach et al. 2021), but objects studied in both X-ray and radio tend to bias toward black holes, as neutron star accretion dynamics are more complicated than black holes, and the periods of outburst are shorter.

If all ULXs are either super-Eddington stellar-mass black holes or neutron stars, they are in a significantly different accretion state than the sub-Eddington systems described in the previous paragraph. As such, we do not expect ULXs with stellar-mass black holes to display the same luminosity correlations. Nevertheless, we are inspired by the above to investigate whether, in the super-Eddington regime, there are radio signatures that might discriminate between black hole and neutron star ULXs. Furthermore, joint radio and X-ray observations of ULXs are often used to distinguish IMBH candidates from stellar-mass XRBs, as well as for discovering active galactic nuclei (AGNs) in low-mass galaxies (e.g., A. E. Reines & A. T. Deller 2012; N. Webb et al. 2012; M. Mezcua et al. 2013, 2018; M. Kim et al. 2015; G. Yang et al. 2016), the assumption being that a ULX would fall along the fundamental plane if powered by an IMBH or a sub-Eddington AGN, and it would fall off the fundamental plane if powered by a super-Eddington XRB. Characterizing the radio properties of known super-Eddington XRBs is therefore helpful for verifying the utility of using the fundamental plane and for eventually quantifying the level to which super-Eddington XRBs (including neutron stars) could be contaminating AGN samples in low-mass galaxies.

Considering the above, in this paper, we perform a radio continuum survey of all known pulsating (i.e., neutron star) ULXs with radio coverage, which currently includes seven of the eight known pulsating ULXs. By focusing on pulsating ULXs, we can be confident in the nature of the compact object. The majority of pulsating ULXs (M82 X-2, NGC 5907 ULX-1, M51 ULX-7, NGC 1313 X-2, and NGC 300 ULX-1) have peak X-ray luminosities well in excess of 5×10^{39} erg s^{-1} (L. Zampieri et al. 2004; P. Kaaret et al. 2006; M. Bachetti et al. 2014; G. L. Israel et al. 2017b, 2017d; S. Carpano et al. 2018; J. van den Eijnden et al. 2018; R. Sathyaprakash et al. 2019; G. A. Rodríguez Castillo et al. 2020; F. Fürst et al. 2023). These sources, while variable, have been observed to be persistently luminous in X-rays over many years (G. Vasilopoulos et al. 2020; C.-P. Hu et al. 2021; F. Fürst et al. 2023). The other two sources often included as pulsating ULXs, located in the Milky Way and Magellanic Clouds, respectively, are Swift J0243.6+6124 (hereafter, Swift J0243) and RX J0209.6-7427, which have peak X-ray luminosities reaching $\sim 2 \times 10^{39}$ erg s^{-1} in outburst (C. A. Wilson-Hodge et al. 2018; A. D. Chandra et al. 2020) and are transient, unlike the extragalactic ULXs in this sample. We stress that the radio properties of some individual pulsating ULXs have already been studied and published (P. Kaaret et al. 2006; M. Mezcua et al. 2013; H. M. Earnshaw 2016; J. van den Eijnden et al. 2018). Our goal in this paper, despite the limited sample size, is to perform the first synthesis study on the radio properties of pulsating ULXs as a population.

This paper is structured as follows. In Section 2, we describe new and archival radio data from the Karl G. Jansky Very Large Array (VLA; R. A. Perley et al. 2011) and the Australia Telescope Compact Array (ATCA; W. E. Wilson et al. 2011). In Section 3, we present our results from each of the seven sources. We then discuss the implications of our results by assessing how the radio properties change with the properties of the neutron star XRB, and how they impact our selection methods for massive black holes via X-ray/radio luminosity ratios. We summarize our findings in Section 4.

2. Observational Data

2.1. Our Sample

Our sample includes seven of the eight neutron star ULXs with observed pulsations. The ULXs included in this study are: M82 X-2, NGC 5907 ULX-1, M51 ULX-7, Swift J0243, NGC 300 X-1, NGC 1313 X-2, and NGC 7793 P13. The sample consists of persistent extragalactic systems, except for Swift J0243. We do not include RX J0209.6-7427, because there is no radio coverage of the source while it was in outburst. Source parameters including R.A. and decl., distances, and peak X-ray luminosities are listed in Table 1.

2.2. Radio Data

The archival radio continuum data used in this study came from the VLA and the ATCA. The VLA data were taken primarily in C band (4.0–8.0 GHz), with the exception of NGC 5907 ULX-1, which has additional *X*-band (8.0–12.0 GHz) data. ATCA observations cover the *C* and *X* bands simultaneously.

Three of the sources have ATCA data: NGC 1313 X-2 (Project Code: C2588; PI: Cseh), NGC 300 ULX-1 (Project Code: C3050; PI: Soria and Project Code: C3120; PI: Urquhart), and NGC 7792 P13 (Project Code: C3547; PI: Dage). All observations were taken with the extended 6 km configuration. NGC 1313 X-2 and N7792 P13 were taken in two basebands centered at 5.5 and 9.0 GHz, each with 2.0 GHz of bandwidth. Data for NGC 1313 X-2 were taken on 2011 December 16, with a total of 21.16 hr on the source, and data for NGC 7792 P13 were taken on 2023 December 16, with 10.42 hr on P13. These data were flagged and calibrated using standard procedures within the Common Astronomy Software Application (CASA) version 5.6.3 (CASA Team et al. 2022) and imaged using the `tclean` algorithm with Briggs weighting scheme and a robust setting of 1. Details of the observation and data processing of NGC 300 are described in R. Urquhart et al. (2019).

The other sources—M82 X-2 (AL629; PI: Lang), NGC 5907 ULX-1 (12A-183; PI: Mezcua and 19A-148; PI: Middleton), M51 ULX-7 (12A-287; PI: Miller), and Swift J0243 (17B-406 and 17B-420; PI: van den Eijnden)—were observed with the VLA in A or B configuration. We do not reanalyze the published observations of AL629 (M82 X-2), 12A-183 (NGC 5907 ULX-1), 17B-406 (Swift J0243), and 17B-420 (Swift J0243); instead, we adopt values from P. Kaaret et al. (2006), M. Mezcua et al. (2013), and J. van den Eijnden et al. (2018). The unpublished data of NGC 5907 ULX X-1 for program ID 19A-148 were observed four times with *X*-band receivers (8.0–12.0 GHz) in A configuration with 41.4 minutes on target. The unpublished archival C-band (4.0–8.0 GHz) data

Table 1
Neutron Star ULX Radio and X-Ray Luminosities

Source	R.A. (h:m:s)	Decl. (°:′:″)	Distance (Mpc)	Radio Program ID	Observation Date	Flux Density (μJy)	Peak X-Ray Luminosity (1–10 keV erg s^{-1})
M82 X-2	09:55:51.04	69:40:45.49	3.6	VLA AL629[α]	2005 Jan 29	2.9 ± 0.1 mJy (8.5 GHz)	9.0×10^{39}
NGC 5907 ULX-1	15:15:58.62	56:18:10.3	17.1	VLA 12A-183[β]	2012 May 30	<12.9 (5.0 GHz)	7.6×10^{40}
				VLA 19A-148	2019 March 5	<18.3 (9.0 GHz)	
					2019 April 30	<15.3	
					2019 May 30	<29.4	
					2019 July 1	<22.2	
M51 ULX-7	13:30:01.098	47:13:42.33	8.58	VLA 12A-287	2012 June 2	<53.4 (6.0 GHz)	4.0×10^{39}
Swift J0243	02:43:40.43	61:26:03.76	5.2×10^{-3}	VLA 17B-406[γ]	2017 Oct 10	<12 (6.0 GHz)	8.7×10^{38}
					2017 Nov 8	77.1 ± 4.2	
				VLA 17B-420[γ]	2017 Nov 15	92.6 ± 3.8	
					2017 Nov 21	63.4 ± 4.3	
					2017 Nov 23	55.3 ± 4.4	
					2017 Nov 28	34.8 ± 4.0	
					2017 Dec 2	24.7 ± 4.5	
					2018 Jan 9	21.3 ± 4.0	
NGC 300 ULX-1	00:55:04.86	37:41:43.7	1.88	ATCA C3050	2015 Oct 21–23	<14.4 (5.0 GHz)	2.4×10^{39}
NGC 1313 X-2	03:18:22.18	-66:36:03.3	3.7	ATCA C2588	2011 Dec 16	<124.5 (5.0 GHz)	6.0×10^{39}
NGC 7793 P13	23:57:50.9	32:37:26.6	3.83	ATCA C3547	2023 Dec 16	<36.2 (5.0 GHz)	3.7×10^{39}

Note. Program IDs marked with α mean that we adopt the published radio luminosity from P. Kaaret et al. (2006), β is the published radio luminosity from M. Mezcua et al. (2013), and γ are the radio luminosities measured and published by J. van den Eijnden et al. (2018).

from M51 ULX-7 in 2012 were taken in B configuration with 10.6 minutes on the source. Each epoch was split into two 2.0 GHz baseband images, centered at 9.0 and 11.0 GHz and 5.0 and 7.0 GHz, respectively. All flagging, calibration, and imaging was done using CASA version 5.6.2, using the Briggs weighting scheme of robustness 1 to efficiently balance the sensitivity and resolution of the image.

Observations that resulted in nondetections are reported in Table 1 as 3σ upper limits, where 1σ denotes the rms noise in a source-free region surrounding the target location.

2.3. X-Ray Data

While all of the pulsating ULXs have been well studied over the long term with a number of X-ray observatories, we require X-ray luminosities in the 1–10 keV range for the purposes of the fundamental plane relation. Thus, we perform a new extraction of one X-ray spectrum per source and model it with the best-fit model reported by the relevant literature, to calculate the 1–10 keV fluxes.

The long-term monitoring of these sources has enabled a unique study of long-term variability in extragalactic X-ray sources. While sources like Swift J0243 and NGC 300 ULX-1 display transience (an outburst followed by a decay and subsequently not being detected above the Eddington limit), M82 X-2, NGC 1313 X-2, NGC 7793 P13, M51 ULX-7, and NGC 5907 ULX-1 all show long-term order-of-magnitude changes in flux (e.g., L. J. Townsend & P. A. Charles 2020; A. Robba et al. 2021; F. Fürst et al. 2023 and references therein).

Given that our goal is to assess whether a neutron star ULX could confuse a search for an IMBH, we select one X-ray observation of each source when it is near its peak X-ray luminosity, extract the background-subtracted source counts, and model the spectrum. We note that this is already an issue with the hard-state condition for using the fundamental plane of radio/X-ray correlation to estimate mass; however, most extragalactic ULXs do not have of years of monitoring in X-ray and may have only been observed once above the Eddington limit.[10]

We further note that none of these X-ray observations are simultaneous with radio, and there are no instances where the archival X-ray data are strictly simultaneous with the archival (or new) radio data. Simultaneity is a requirement for using the fundamental plane. However, many ULXs are being discovered with archival data searches (e.g., D. J. Walton et al. 2022), and many ULX sources again do not have the luxury of widespread radio studies.

For the purposes of this study, it is illustrative enough to choose one bright X-ray observation out of the many available, but the short timescale of X-ray variability that is observed in most of these pulsating ULXs should serve as an additional caution for invoking the assumptions of the fundamental plane on a ULX where little is known.

The choice of models for X-ray spectra is also an interesting discussion, as the shape and best-fit parameters of the spectral model can directly influence the measured X-ray flux. However, the ability to perform detailed modeling of the X-ray spectral shape is a function of the sensitivity of the instrument, as well as the number of photons (i.e., both the distance to the source and the intrinsic luminosity coming from the source). The pulsating ULXs in the present sample are both relatively nearby and extremely luminous, enabling very detailed modeling (and therefore a better understanding) of their X-ray spectral states, via observatories such as NuSTAR and XMM-Newton, but many other ULXs do not share this luxury.

With these caveats in mind, we perform the X-ray analysis as follows.

[10] The discussion of variability and transience in ULXs when they are not well monitored is an ongoing discussion out of scope of this work, but see M. Brightman et al. (2023), K. Atapin et al. (2024), and K. C. Dage et al. (2021) for a discussion of how the transient/variable nature of ULXs impacts our overall understanding of the population.

Table 2
Best-fit Parameters and Fluxes for ULXs Fit with `tbabs*tbabs*diskbb` or `tbabs*tbabs*powerlaw`

Source	α	$N_{\rm H}$ ($\rm cm^{-2}$)	kT (keV)	Γ	Norm.	Flux ($\rm erg\ s^{-1}\ cm^{-2}$)
M82 X-2	$0.35\ ^{+0.10}_{-0.05}$	2.85 ± 0.20	$2.48\ ^{+0.36}_{-0.28}$	⋯	$2.4 \pm 0.2 \times 10^{-2}$	$5.8 \pm 0.1 \times 10^{-12}$
M51 ULX-7	⋯	⋯	⋯	1.5 ± 0.1	$6.7 \pm 0.4 \times 10^{-5}$	$4.5 \pm 0.1 \times 10^{-13}$
NGC 1313 X-2	0.5	0.12 ± 0.02	1.6 ± 0.1	⋯	0.5 ± 0.1	$3.7 \pm 0.1 \times 10^{-12}$
NGC 7793 P13	0.5	0.06 ± 0.02	⋯	1.2 ± 0.1	$3.9 \pm 0.2 \times 10^{-3}$	$2.1 \pm 0.1 \times 10^{-12}$
NGC 300 ULX-1	⋯	⋯	⋯	1.2 ± 0.1	$6.3 \pm 0.5 \times 10^{-4}$	$6.8 \pm 1.0 \times 10^{-12}$
NGC 300 ULX-1	⋯	⋯	2.3 ± 0.4	⋯	$1.2 \pm 0.4 \times 10^{-2}$	$5.8 \pm 0.8 \times 10^{-12}$
NGC 5907 ULX-1	⋯	$1.16^{+1.25}_{-0.89}$	⋯	1.8 ± 0.9	$6.1 \pm 4.1 \times 10^{-4}$	$2.9 \pm 1.0 \times 10^{-12}$

All of the sources where we use an observation from Swift/X-Ray Telescope (XRT) were extracted via the build products page hosted by Swift[11] (P. A. Evans et al. 2009), using HEASOFT v6.32. All of the Chandra (M. C. Weisskopf et al. 2000) observations we used were reprocessed with CHANDRA REPRO, using CIAO version 4.15 (A. Fruscione et al. 2006) and HEASOFT v6.31.1. All of the background-subtracted source spectra were extracted with SPECEXTRACT and binned by 20 counts. The extraction source regions are discussed on a case-by-case basis below, and the background for all sources was extracted by placing six of the same size regions around the source region, making small shifts to avoid any nearby point sources while still sampling the nearby background. All spectra were fitted with XSPEC 12.13.0c (K. A. Arnaud 1996), abundances from J. Wilms et al. (2000), and photoelectric cross sections from D. A. Verner et al. (1996). For all sources, we obtained line-of-sight neutral hydrogen density ($N_{\rm H}$) from Chandra[12] and performed fits with `tbabs` fixed to this value. For all, we ignored any bad bins. For the Chandra observations, we fit within the 0.5–8.0 keV range, binned by 20 with χ^s statistics. As the Swift observations had total source counts an order of magnitude lower than the Chandra observations, due to lower instrument sensitivity and overall lower exposure times, we fit these with W-stat (W. Cash 1979), binned by 1, and used Anderson–Darling as the test statistic. We fit the Swift photon-counting (PC) mode observations in the 0.3–10 keV regime and the Swift windowed timing (WT) mode in the 0.7–10 keV range. All errors reported are at the 90% interval.

For M82 X-2, we selected ObsID 16580 (PI: Margutti; 50 ks; 2014 February 3; ACIS-S), based on a previous study by M. Brightman et al. (2016). We used a source extraction region of 1.″5. As discussed by M. Brightman et al. (2016), this was an on-axis observation that was affected by pileup, and the overall fit statistics indicated that a blackbody disk (K. Mitsuda et al. 1984) was the best-fit model for this source. We performed a fit with the model `pileup*tbabs*tbabs*diskbb`, keeping the first `tbabs` component fixed to the line-of-sight $N_{\rm H}$, as discussed above, and leaving the second column density free to measure intrinsic absorption. To obtain the 1–10 keV flux, we used `cflux`, removing the pileup model and freezing the fit parameters. Our fit values are reported in Table 2. The fit statistic is 239.81, with 271 bins and a null hypothesis probability of 8.83×10^{-1} with 267 degrees of freedom. Within errors, our fit parameters are consistent with those of M. Brightman et al. (2016).

For M51 ULX-7, the source was marginally off-axis and we extracted with a 5″ region. We selected ObsID 13814 (2012 September 20; 190 ks; PI: Kuntz; ACIS-S). The source count rate was not high enough to have an issue with pileup. H. M. Earnshaw (2016) reports that this source is best fit with a single-power-law model. We initially attempted a second free absorbing column, but the best-fit value was consistent with zero, so we omitted it and only fit `tbabs*powerlaw`, with `tbabs` frozen to the line-of-sight value.

Our fit values are reported in Table 2. The fit statistic was 220.16/205, with a null hypothesis probability of 1.81×10^{-1} with 202 degrees of freedom. This is consistent with the results of H. M. Earnshaw (2016).

NGC 1313 X-2 was off-axis and we used a 10″ extraction region. We used ObsID 2950 (2002 December 13; 20 ks; PI: Murray; ACIS-S). Due to the high source count rate, we modeled pileup with the α parameter frozen to 0.5.[13] Fitting with an absorbed `diskbb` model provided better fit statistics (216.34/208) than a power law (237.4/208). Our fit values are reported in Table 2. Our fit parameters are consistent with J. J. E. Kajava & J. Poutanen (2008).

We modeled NGC 7793 P13 similarly to NGC 1313 X-2, which was also off-axis and affected by pileup. We used ObsID 3954 (2003 September 6; PI: Pannuti; 50 ks; ACIS-S). We used an extraction region of 7″. Once again, α was frozen to 0.5. The fit statistics for a disk (355.41/221 bins) were worse than a power law (244.1/221 bins), so we fit `pileup*tbabs*tbabs*powerlaw`. The fit values are reported in Table 2. We note this fit is consistent with G. L. Israel et al. (2017c).

For NGC 300 ULX-1, we used ObsID 00049834010, which was observed by Swift in PC mode for 5194 s on 2017 April 22 (PI: Binder). B. Binder et al. (2018) report 1–10 keV fluxes and fit 11 Swift observations simultaneously. We selected the longest observation, ID 00049834010, and fit it with a simpler absorbed power-law model. We did not use a second unfixed absorbing column, as it was consistent with zero, and we fixed our line-of-sight value to $3.08 \times 10^{22}\ \rm cm^2$. For comparison, we also fit an absorbed blackbody disk model, and the fits are reported in Table 2. The Anderson–Darling fit statistics for the power-law model are −6.96 using 325 bins and for the diskbb model are −6.05 using 325 bins. We also note that B. Binder et al. (2018) found that the X-ray luminosity was consistent across their 11 observations, and it is also consistent, within uncertainties, with the ones we have obtained by modeling with simpler spectra.

For NGC 5907, we used ObsID 00032764009 (PI: Pintore), taken on 2018 February 14, using Swift with PC mode for a 2266 s exposure. G. L. Israel et al. (2017a) fit their Swift observations with the tbabs*bknpowerlaw model, with absorption, energy cutoff, and both power laws fixed. When we fit

[11] https://www.swift.ac.uk/
[12] https://cxc.harvard.edu/toolkit/colden.jsp
[13] https://cxc.harvard.edu/ciao/download/doc/pileup_abc.pdf

Table 3
Observations and 1.0–10 keV Fluxes for Swift J0243

ObsID	Exp. Length (s)	Obs. Date	Flux ($\times 10^{-8}$ erg s^{-1} cm^{-2})
00010336007	1931	2017-10-10	0.94 ± 0.03
00010336022	1054	2017-11-09	26.89 ± 0.01
00010336025	1019	2017-11-15	16.31 ± 0.01
00010336031	989	2017-11-27	7.24 ± 0.01
00010336033	1029	2017-12-01	4.82 ± 0.01
00010467007	899	2018-01-02	1.60 ± 0.01
00010467008	1034	2018-01-13	1.10 ± 0.01

with their fixed parameter model and cflux, we recover a 1–10 keV flux of $2.19 \pm 0.48 \times 10^{-12}$. For the simpler model of `tbabs*tbabs*powerlaw`, the Anderson–Darling test was −5.44, and we report the fits in Table 2.

Swift J0243 was observed seven times in outburst, in WT mode (PIs: Heinz, Kennea, and Wolff). J. van den Eijnden et al. (2018) fit TBABS*BBODYRAD*POWERLAW, cutting off energies below 0.7 keV to all observations except 00010467008, which was fit with TBABS*(POWERLAW. Because we are only interested in the 1–10 keV fluxes, and J. van den Eijnden et al. (2018) have already performed detailed X-ray spectroscopy, after ensuring that we recover their best-fit model parameters, we use CFLUX to obtain the 1–10 keV fluxes, which are presented in Table 3.

J. van den Eijnden et al. (2018) also interpolated X-ray fluxes for radio observations taken on 2017 November 21 and 2017 November 23 with log-linear interpolation. We also performed log-linear interpolation; for 2017 November 21, we interpolate the 1–10 keV X-ray flux to be 1.01×10^{-7} erg s^{-1} cm^{-2}, and for 2017 November 23, we interpolate a 1–10 keV X-ray flux of 8.87×10^{-8} erg s^{-1} cm^{-2}.

3. Results and Discussion

We describe individual sources and their radio/X-ray properties below. To briefly summarize, the only radio-detected source is the Galactic ULX Swift J0243 (J. van den Eijnden et al. 2018). A radio counterpart is also detected from M82 X-2, but this likely arises from an H II region and not the ULX (see Section 3.1).

Before discussing each source, we first comment that radio counterparts to ULXs are relatively rare. When radio emission is detected, it usually appears as a "radio bubble," which is an extended nebular feature that emits optically thin synchrotron radiation, likely associated with an active or past outflow shocking the nearby interstellar medium (M. W. Pakull et al. 2010; R. Soria et al. 2010; D. Cseh et al. 2014, 2015a; G. E. Anderson et al. 2019; R. Urquhart et al. 2019). Typical bubble sizes range from 30 to 300 parsecs (C. T. Berghea et al. 2020). No pulsating ULX (including Swift J0243) has yet to be linked to radio bubbles. Radio emission from jets is also possible, but so far has only been seen in a handful of ULXs (M. Mezcua et al. 2013; M. J. Middleton et al. 2013; D. Cseh et al. 2015b; G. Yang et al. 2016).

3.1. M82 X-2

M82 X-2 was the first detected neutron star ULX, confirmed through X-ray pulsed emission from NuSTAR in 2014 (M. Bachetti et al. 2014). The source has an orbital period ∼2.5 days (M. Bachetti et al. 2022). The predicted magnetic field strength is $B \approx 10^{12}$ G (M. Bachetti et al. 2014; K. Y. Eksi et al. 2015; S. S. Tsygankov et al. 2016), but may be as low as $<10^{9}$ G (W. Kluzniak & J.-P. Lasota 2015). The peak X-ray luminosity of the source is 2×10^{40} erg s^{-1} in the 0.3–10 keV band (M. Bachetti et al. 2014).

Previous radio flux density measurements were made using the VLA in 2005 (VLA/AL629; PI: Lang); P. Kaaret et al. (2006) reported a significant (∼1 mJy) detection near the position of the ULX, and we adopt this value for subsequent analysis in this paper. As seen in their Figure 8, the ULX source is quite offset from the center of the radio contours. We also note that a source was detected at the position of the ULX in an eMERLIN survey (M. A. Gendre et al. 2013) and classified as an H II region (source 16 or 42.20 + 59.1 in their Table 2). If we take the detection at face value, it corresponds to a radio luminosity of 1.3×10^{35} erg s^{-1}, which is unreasonably luminous to expect from an XRB, but typical for an H II region (M. A. Gendre et al. 2013). While M82 X-2 is located in an extremely dusty part of the host galaxy, James Webb Space Telescope observations may be able to provide better insight to the ULX's environment. Regardless, this underscores the impact that background star formation can have on radio measurements of XRBs.

3.2. NGC 5907 ULX-1

NGC 5907 ULX-1 was observed in radio by M. Mezcua et al. (2013), who published an upper limit (<0.020 mJy) in a 5.0 GHz VLA observation (VLA/12A-183; PI: Mezcua). We adopt this upper-limit value for this paper. They used the fundamental plane of black hole activity to infer that the compact object is a black hole with a mass upper limit of $3 \times 10^{3}\,M_{\odot}$. More recently, X-ray pulsations have been detected with a 1.43 s spin period and a peak X-ray luminosity of 5×10^{40} erg s^{-1} (G. L. Israel et al. 2017b), clearly ruling out a black hole scenario.

3.3. M51 ULX-7

M51 has been subjected to multiple observational campaigns at various wavelengths due to its high star formation rate and large number of X-ray sources (R. E. Kilgard et al. 2005). M51 ULX-7 is a pulsar ULX system at a distance of 8.6 ± 0.1 Mpc (K. B. W. McQuinn et al. 2016). The neutron star has a 2.8 s spin period and an orbital period of ∼2 days (G. A. Rodríguez Castillo et al. 2020). The system has a peak X-ray luminosity of $\sim 10^{40}$ erg s^{-1} (G. A. Rodríguez Castillo et al. 2020) and was discovered to exhibit superorbital modulations from its Swift/XRT light curves at a period of 38 days (M. Brightman et al. 2020; G. Vasilopoulos et al. 2020).

Previous radio observations of M51 ULX-7 are limited. Observations of ULX-7 have been published in H. M. Earnshaw (2016) using *L*-band (1.0–2.0 GHz) data from VLA/11A-142 (PI: Hughes). The source was not detected during this observation, measuring an upper limit of <87 μJy at 1.5 GHz. In this study, we use archival *C*-band (4.0–8.0 GHz) data from VLA/12A-287 (PI: Miller) on 2012 June 2, measuring an upper limit of <53 μJy at 6.0 GHz.

3.4. Swift J0243

Swift J0243 is one of the few super-Eddington sources in our Galaxy. There have been many previously reported distance values, from ∼2.5 to 6 kpc (I. Bikmaev et al. 2017; J. van den Eijnden et al. 2018; Y. Zhang et al. 2019; P. Reig et al. 2020),

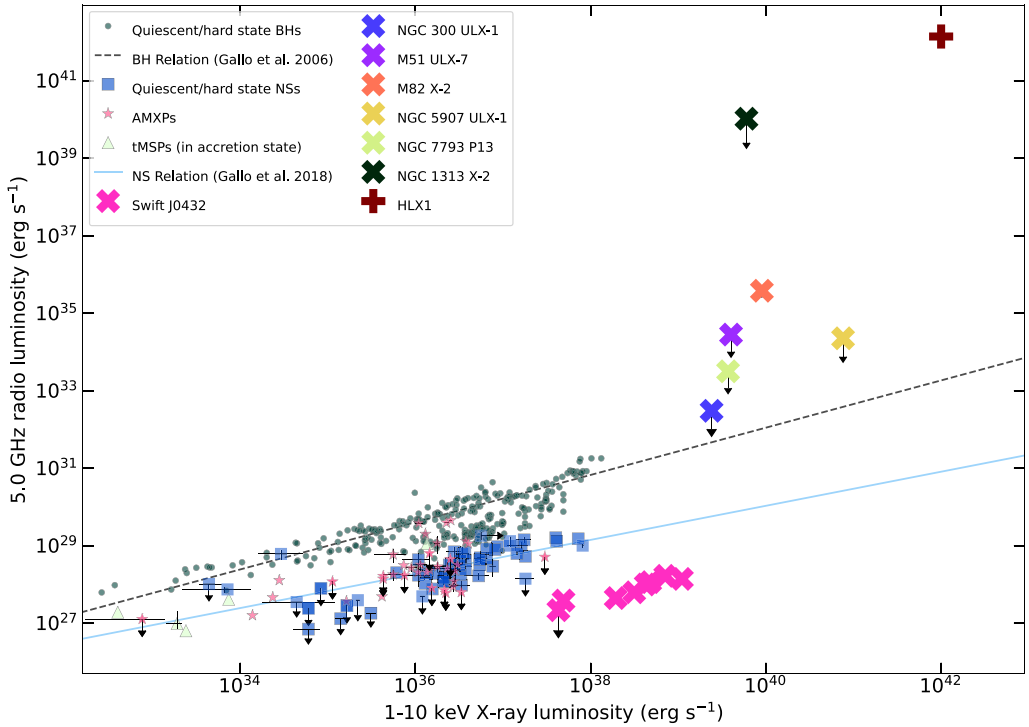

Figure 1. The radio/X-ray luminosity correlation plane for accreting compact objects adapted from A. Bahramian et al. (2018). Quiescent/hard-state black holes are indicated by the dark green circles. We include the following neutron star populations: quiescent/hard-state neutron stars as blue squares and accreting millisecond X-ray pulsars (AMXPs) and transitional millisecond pulsars (tMSPs) as pink stars and mint triangles. The neutron star ULXs in our sample are indicated by large "X"s. We also include HLX-1 (D. Cseh et al. 2015b) for comparison. The gray line represents the best-fit regression for black holes from E. Gallo et al. (2006), while the blue line represents the proposed correlation for hard-state neutron stars from E. Gallo et al. (2018).

and most recently from the latest Gaia DR3 catalog, $5.5^{+0.4}_{-0.3}$ kpc (Gaia Collaboration 2022). For this study, we use a distance of 5.2 kpc, adopting the lower limit similar to J. van den Eijnden et al. (2018). Swift J0243 was first discovered by Swift's Burst Alert Telescope (N. Gehrels et al. 2004) in 2007 through a giant outburst (S. B. Cenko et al. 2017) and was found to exhibit X-ray pulsations with a period of 9.86 s (A. Bahramian et al. 2017; J. A. Kennea et al. 2017; C. A. Wilson-Hodge et al. 2018), establishing the compact primary to be an accreting neutron star. Later optical spectroscopic observations of Swift J0243 showed it to have a Be counterpart, making it a part of a special class of high-mass XRBs, Be/X-ray sources (P. Reig et al. 2020) with a strong magnetic field ($B \geqslant 10^{12}$ G; V. Doroshenko et al. 2018).

Swift J0243 is one of the few ULX sources with multiple high-quality quasi-simultaneous radio and X-ray observations. J. van den Eijnden et al. (2018) followed the source from outburst to quiescence over eight *C*-band (4.0–8.0 GHz) VLA (17B-406 and 17B-420; PI: van den Eijnden) and seven Swift/XRT observations. They observed radio and X-ray emission that was correlated, but seen at a much lower level than neutron stars with low magnetic fields. Thus, while high magnetic fields apparently do not inhibit jet launching in ULXs, they cause the jets to be much fainter in radio. From J. van den Eijnden et al. (2018), we adopt 5.0 GHz radio and measure 1–10 keV X-ray luminosities to place these epochs on the radio/correlation plane in Figure 1.

3.5. NGC 300 ULX-1

NGC 300 ULX-1 was initially thought to be a supernova, SN2010da (R. Khan et al. 2010), and later was categorized as a Wolf Rayet/black hole XRB system (S. Carpano et al. 2007), until it was discovered to have X-ray pulsations through NuSTAR (F. A. Harrison et al. 2013) and XMM-Newton (L. Strüder et al. 2001), with a strong periodic modulation (31.6s) in the X-ray flux (S. Carpano et al. 2018). It reaches a peak X-ray luminosity of 5×10^{39} erg s^{-1} (S. Carpano et al. 2018).

For our analysis, we reduced archival ATCA observations from 2014, with the pointing center 2″ from the NGC 300 ULX-1 system (Project Code: C3050; PI: Soria and Project Code: C3120; PI: Urquhart). We measure a flux density upper limit of <11 μJy at 5.0 GHz, and we adopt the X-ray flux shown in Table 1.

3.6. NGC 1313 X-2

NGC 1313 X-2 has a 1.5 s spin period and a peak X-ray luminosity of 2×10^{40} erg s^{-1} (R. Sathyaprakash et al. 2019). While it was observed by ATCA in 2011 (Project Code: C2588; PI: Cseh), the center of the field pointed approximately 30″ from the pulsating ULX source. The ULX is far enough off the pointing center that it is more challenging to obtain a meaningful 3σ upper limit, with our best constraint being <124 μJy at 5.0 GHz.

3.7. NGC 7793 P13

NGC 7793 P13 was first identified in 2003 as an X-ray source in a Chandra X-ray Telescope survey of NGC 7793 (T. G. Pannuti et al. 2006). Previous Swift/XRT monitoring of P13 in 2010 showed a range of $L_x \sim 3$–5×10^{39} erg s^{-1} (C. Motch et al. 2014) and later found a peak at luminosities of 10^{40} erg s^{-1} (G. L. Israel et al. 2017d). It is the fastest-pulsating

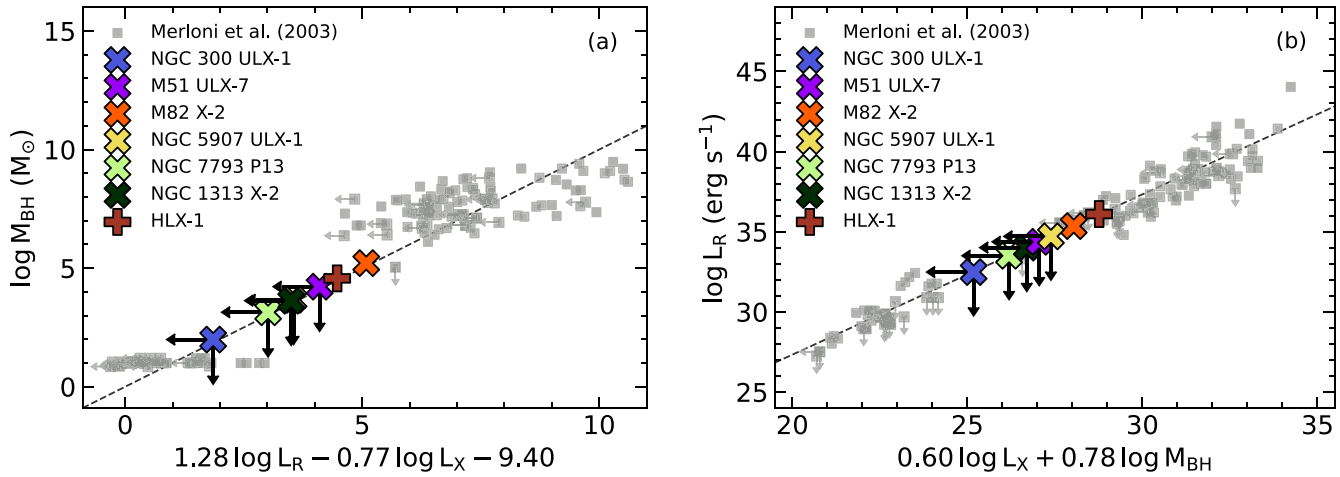

Figure 2. Our sample of extragalactic neutron star ULXs (shown by cross symbols) projected onto the fundamental plane, showing the result if one were to naively estimate "black hole" masses via the radio and X-ray luminosities/limits (here, we have used Equation (15) of A. Merloni et al. 2003). The gray symbols show XRBs and AGNs from A. Merloni et al. (2003), and the dashed line shows their best-fit function. Since it is common for studies to employ joint radio and X-ray observations to search for AGNs in low-mass galaxies, this figure illustrates the parameter space where neutron star ULXs could potentially masquerade as IMBH/low-mass AGNs. (a) A projection of the fundamental plane with black hole mass as the dependent variable. The radio and X-ray luminosities/limits of our sample have led to erroneous mass estimates or upper limits of $\sim 10^2$–$10^5 M_\odot$. (b) The same data projected onto the typical view of the fundamental plane. Note: the radio counterpart to M82 X-2 is likely from a coincident H II region, but we depict it as a radio detection here, to illustrate how such a misidentification would incorrectly imply a $\approx 10^5\ M_\odot$ IMBH. The Galactic source Swift J0243 is not included in this figure, as the fundamental plane correctly predicts this source cannot be a black hole (see Section 3.8). For comparison, we also include HLX-1 (as a plus symbol), as measured in X-ray and radio by D. Cseh et al. (2015b).

ULX, with a spin period of 0.42 s. It was observed with ATCA in 2023 December (ATCA/C3547; PI: Dage), with a 3σ upper-limit radio flux density of $<36\ \mu$Jy at 5.0 GHz.

3.8. Do Neutron Star ULXs Contaminate the Fundamental Plane?

One objective of this study is to identify whether ULXs that are known neutron stars could act as contaminants to black hole candidates selected through the radio/X-ray luminosity correlation and/or the fundamental plane—i.e., if their identification was not secure as neutron stars, could they be mistaken as massive black hole candidates based off their X-ray and radio emission?

First, a strong word of caution is that the radio/X-ray luminosity correlation, and by extension the fundamental plane, are derived from hard-state XRBs and their supermassive analogs (E. Gallo et al. 2003, 2018; A. Merloni et al. 2003; H. Falcke et al. 2004; M. Coriat et al. 2011; K. Gültekin et al. 2019; P.-X. Shen & W.-M. Gu 2020). ULXs have their own distinct spectral states (J. C. Gladstone et al. 2009; A. D. Sutton et al. 2013; R. Urquhart & R. Soria 2016). Unless a ULX is a sub-Eddington IMBH, it is not expected to fit along the radio/X-ray luminosity correlation. As such, we stress that there is no physical motivation to place a known pulsating ULX onto the radio/X-ray luminosity correlation or onto the fundamental plane. Rather, the exercise here is to assess the level to which pulsating ULXs could masquerade as black holes during joint radio/X-ray studies, should one not be aware of the nature of the compact object. We also note that many of the nontransient ULX sources in our sample are highly variable, on the scale of an order of magnitude in X-ray flux (e.g., F. Fürst et al. 2021), which would introduce extra scatter in radio/X-ray luminosity correlations and in the fundamental plane. Ideally, radio and X-ray observations would be taken taken simultaneously, which was unfortunately not feasible for most objects in our sample, with the exception of the J. van den Eijnden et al. (2018) monitoring campaign on Swift J0243.

With the above caveats in mind, if one were to blindly place our sample onto the fundamental plane (Figure 2, using masses estimated via Equation (15) of A. Merloni et al. 2003), the results would be largely misleading. The only exception is the Galactic ULX Swift J0243, where the fundamental plane predicts a mass of $10^{-4}\ M_\odot$, which is clearly inconsistent with a black hole. At the other extreme, an egregious error could occur if one were to not recognize the radio counterpart to M82 X-2 as a background H II region (M. A. Gendre et al. 2013), in which case the fundamental plane would suggest a $\sim 10^5 M_\odot$ IMBH. One could envision this type of mistake happening if a system like M82 X-2 were part of a larger sample derived from crossmatching X-ray and radio catalogs (a scenario where investigating misidentifications on an individual basis is often not feasible).

For the other five ULXs in our sample with radio nondetections, the fundamental plane suggests black holes with mass upper limits ranging from $\lesssim$50–10,000 $M_\odot$. The severity of this (misleading) calculation on the final interpretation depends on the context of the specific study. Nevertheless, Figure 2 illustrates the parameter space where misinterpretation of pulsating ULXs would contaminate the fundamental plane.

On the other hand, if one compares our sample only to other stellar-mass compact objects, neutron star ULXs do appear distinguishable from other objects in the radio/X-ray luminosity correlation (see Figure 1), although this is not an appropriate comparison, since stellar-mass systems on the Fundamental Plane should not be above Eddington, as they would no longer be in the hard state. Our sample of neutron star ULXs fall into two classes in Figure 1, a lower-X-ray-luminosity source detected in radio (Swift J0243), and higher-X-ray-luminosity sources not detected in radio beyond the background emission. However, given the persistent ULXs are all upper limits in radio, it is possible that the true measurements may be broadly consistent with Swift J0243.

A major caveat, of course, is that we cannot compare the location of our pulsating ULXs to ULXs known to be powered

by stellar-mass black holes (since it is unclear if nonpulsating ULXs are powered by black holes or neutron stars). Nevertheless, it is worth commenting that the detected radio emission from the Galactic ULX Swift J0243 (J. van den Eijnden et al. 2018) is significantly less luminous than the radio emission from hard-state neutron stars from E. Gallo et al. (2018). As discussed in J. van den Eijnden et al. (2018), this is likely due to the source's high magnetic field.

One of the leading explanations for how neutron star ULXs can produce such a high X-ray luminosity is thanks to a high magnetic field strength (e.g., M. Brightman et al. 2018). If this is indeed the case, then it is not a surprise that the (more distant) neutron star ULXs were not detected in radio.

4. Summary and Conclusions

We have analyzed radio observations of neutron star ULXs in conjunction with existing studies to complete the largest radio study of neutron star ULXs. We combined the radio observations with published X-ray luminosities to assess whether neutron star ULXs are likely to fill the same radio/X-ray parameter space as bona fide IMBHs. Our results are as follows:

1. In X-ray/radio parameter space, Swift J0243 is highly dissimilar to the other pulsating ULXs, both because it is actually detected in radio (although it is also the only Galactic system) and also because it is much fainter in X-ray. This suggests that Swift J0243 may be dissimilar from the more luminous extragalactic population of neutron star ULXs.
2. If one were to take M82 X-2's radio counterpart at face value, it would imply a rather massive black hole. However, as reported by M. A. Gendre et al. (2013), the radio counterpart is most likely an H II region near the XRB. This highlights the importance of taking background environments into consideration.
3. NGC 300 ULX-1, NGC 7793 P13, NGC 5907 ULX-1, and M51 ULX-7 occupy a quadrant of L_R/L_X, where, given the intrinsic scatter in the relation, one could misappropriate the radio upper limit to infer a mass range consistent with an IMBH. We thus urge extreme caution when using L_R/L_X to calculate black-hole-mass upper limits based on radio nondetections.

With current facilities, we do not detect a significant radio counterpart to any extragalactic neutron star ULX. Although we are mainly presenting upper limits in this study, there are are two major conclusions to be drawn: the first is that until a larger sample of neutron star ULXs is uncovered, or we have increased capabilities from facilities such as the next-generation VLA[14] and Square Kilometer Array,[15] our study strongly suggests that, once background star formation has been properly accounted for, it is possible to use radio detections to differentiate neutron star ULXs from massive black hole ULXs. In contrast to our sample of pulsating ULXs, the study by D. Cseh et al. (2015b) of HLX-1 demonstrates that, with due caution, L_R/L_X can be successfully used to interpret a radio counterpart to a ULX and provide a complementary mass estimate.

[14] https://ngvla.nrao.edu/
[15] https://www.skao.int/

Our second conclusion is that we urge caution with the implementation of L_R/L_X, particularly for sources that are not detected in radio. Our results further demonstrate the incompatibility of L_R/L_X and ULXs in the super-Eddington state.

Acknowledgments

The authors thank Eric Koch and Rupali Chandar for helpful discussion. K.C.D. acknowledges support for this work provided by NASA through the NASA Hubble Fellowship grant HST-HF2-51528 awarded by the Space Telescope Science Institute, which is operated by the Association of Universities for Research in Astronomy, Inc., for NASA, under contract NAS526555. This work was partially supported by the Australian government through the Australian Research Council's Discovery Projects funding scheme (DP200102471). R.M.P. and J.D.P. acknowledge support from the National Science Foundation under grant AST-2206123. The Australia Telescope Compact Array is part of the Australia Telescope National Facility (https://ror.org/05qajvd42), which is funded by the Australian Government for operation as a National Facility managed by CSIRO. We acknowledge the Gomeroi people as the Traditional Owners of the Observatory site. This work has made use of data supplied by the UK Swift Science Data Center at the University of Leicester.

Facilities: VLA, ATCA, Chandra, Swift.

Software: astropy (Astropy Collaboration et al. 2013), CASA (CASA Team et al. 2022), matplotlib (J. D. Hunter 2007), NumPy (C. R. Harris et al. 2020), pandas (W. McKinney 2010), CIAO (A. Fruscione et al. 2006), XSPEC (K. A. Arnaud 1996).

ORCID iDs

Teresa Panurach https://orcid.org/0000-0001-8424-2848
Kristen C. Dage https://orcid.org/0000-0002-8532-4025
Ryan Urquhart https://orcid.org/0000-0003-1814-8620
Richard M. Plotkin https://orcid.org/0000-0002-7092-0326
Jeremiah D. Paul https://orcid.org/0000-0003-0040-3910
Arash Bahramian https://orcid.org/0000-0003-2506-6041
McKinley C. Brumback https://orcid.org/0000-0002-4024-6967
Timothy J. Galvin https://orcid.org/0000-0002-2801-766X
Isabella Molina https://orcid.org/0009-0004-4418-0645
James C. A. Miller-Jones https://orcid.org/0000-0003-3124-2814
Payaswini Saikia https://orcid.org/0000-0002-5319-6620

References

Anderson, G. E., Miller-Jones, J. C. A., Middleton, M. J., et al. 2019, MNRAS, 489, 1181
Arnaud, K. A. 1996, in ASP Conf. Ser. 101: Astronomical Data Analysis Software and Systems V (San Francisco, CA: ASP), 17
Astropy Collaboration, Robitaille, T. P., Tollerud, E. J., et al. 2013, A&A, 558, A33
Atapin, K., Vinokurov, A., Sarkisyan, A., et al. 2024, MNRAS, 527, 10185
Bachetti, M., Harrison, F. A., Walton, D. J., et al. 2014, Natur, 514, 202
Bachetti, M., Heida, M., Maccarone, T., et al. 2022, ApJ, 937, 125
Bahramian, A., Kennea, J. A., & Shaw, A. W. 2017, ATel, 10866, 1
Bahramian, A., Miller-Jones, J., Strader, J., et al. 2018, Radio/X-Ray Correlation Database for X-Ray Binaries, v220908, Zenodo, doi:10.5281/zenodo.1252036
Barrows, R. S., Mezcua, M., & Comerford, J. M. 2019, ApJ, 882, 181
Berghea, C. T., Johnson, M. C., Secrest, N. J., et al. 2020, ApJ, 896, 117
Bikmaev, I., Shimansky, V., Irtuganov, E., et al. 2017, ATel, 10968, 1
Binder, B., Levesque, E. M., & Dorn-Wallenstein, T. 2018, ApJ, 863, 141
Blandford, R. D., & Königl, A. 1979, ApJ, 232, 34

Brightman, M., Earnshaw, H., Fürst, F., et al. 2020, ApJ, 895, 127
Brightman, M., Hameury, J.-M., Lasota, J.-P., et al. 2023, ApJ, 951, 51
Brightman, M., Harrison, F. A., Furst, F., et al. 2018, NatAs, 2, 312
Brightman, M., Harrison, F., Walton, D. J., et al. 2016, ApJ, 816, 60
Carpano, S., Haberl, F., Maitra, C., & Vasilopoulos, G. 2018, MNRAS, 476, L45
Carpano, S., Pollock, A. M. T., Wilms, J., Ehle, M., & Schirmer, M. 2007, A&A, 461, L9
CASA Team, Bean, B., Bhatnagar, S., et al. 2022, PASP, 134, 114501
Cash, W. 1979, ApJ, 228, 939
Cenko, S. B., Barthelmy, S. D., D'Avanzo, P., et al. 2017, GCN, 21960, 1
Chandra, A. D., Roy, J., Agrawal, P. C., & Choudhury, M. 2020, MNRAS, 495, 2664
Chomiuk, L., Strader, J., Maccarone, T. J., et al. 2013, ApJ, 777, 69
Corbel, S., & Fender, R. P. 2002, ApJL, 573, L35
Corbel, S., Nowak, M. A., Fender, R. P., Tzioumis, A. K., & Markoff, S. 2003, A&A, 400, 1007
Coriat, M., Corbel, S., Prat, L., et al. 2011, MNRAS, 414, 677
Cseh, D., Kaaret, P., Corbel, S., et al. 2014, MNRAS, 439, L1
Cseh, D., Miller-Jones, J. C. A., Jonker, P. G., et al. 2015a, MNRAS, 452, 24
Cseh, D., Webb, N. A., Godet, O., et al. 2015b, MNRAS, 446, 3268
Dage, K. C., & Kovlakas, K. 2024, arXiv:2407.01768
Dage, K. C., Vowell, N., Thygesen, E., et al. 2021, MNRAS, 508, 4008
Doroshenko, V., Tsygankov, S., & Santangelo, A. 2018, A&A, 613, A19
Earnshaw, H. M. 2016, AN, 337, 448
Eksi, K. Y., Andac, I. C., Cikintoglu, S., et al. 2015, MNRAS, 448, L40
Evans, P. A., Beardmore, A. P., Page, K. L., et al. 2009, MNRAS, 397, 1177
Fabbiano, G. 1989, ARA&A, 27, 87
Fabrika, S. N., Atapin, K. E., Vinokurov, A. S., & Sholukhova, O. N. 2021, AstBu, 76, 6
Falcke, H., Körding, E., & Markoff, S. 2004, A&A, 414, 895
Fender, R. P. 2001, MNRAS, 322, 31
Fruscione, A., McDowell, J. C., Allen, G. E., et al. 2006, Proc. SPIE, 6270, 62701V
Furst, F., Walton, D. J., Harrison, F. A., et al. 2016, ApJL, 831, L14
Fürst, F., Walton, D. J., Heida, M., et al. 2021, A&A, 651, A75
Fürst, F., Walton, D. J., Israel, G. L., et al. 2023, A&A, 672, A140
Gaia Collaboration 2022, yCat, 1355, 0
Gallo, E., Degenaar, N., & van den Eijnden, J. 2018, MNRAS, 478, L132
Gallo, E., Fender, R. P., Miller-Jones, J. C. A., et al. 2006, MNRAS, 370, 1351
Gallo, E., Fender, R. P., & Pooley, G. G. 2003, MNRAS, 344, 60
Gehrels, N., Chincarini, G., Giommi, P., et al. 2004, ApJ, 611, 1005
Gendre, M. A., Fenech, D. M., Beswick, R. J., Muxlow, T. W. B., & Argo, M. K. 2013, MNRAS, 431, 1107
Gladstone, J. C., Roberts, T. P., & Done, C. 2009, MNRAS, 397, 1836
Gültekin, K., King, A. L., Cackett, E. M., et al. 2019, ApJ, 871, 80
Gusinskaia, N. V., Russell, T. D., Hessels, J. W. T., et al. 2020, MNRAS, 492, 1091
Harris, C. R., Millman, K. J., van der Walt, S. J., et al. 2020, Natur, 585, 357
Harrison, F. A., Craig, W. W., Christensen, F. E., et al. 2013, ApJ, 770, 103
Hu, C.-P., Ueda, Y., & Enoto, T. 2021, ApJ, 909, 5
Hunter, J. D. 2007, CSE, 9, 90
Israel, G. L., Belfiore, A., Stella, L., et al. 2017a, Sci, 355, 817
Israel, G. L., Belfiore, A., Stella, L., et al. 2017b, Sci, 355, 817
Israel, G. L., Papitto, A., Esposito, P., et al. 2017c, MNRAS: Lett., 466, L48
Israel, G. L., Papitto, A., Esposito, P., et al. 2017d, MNRAS, 466, L48
Kaaret, P., Feng, H., & Roberts, T. P. 2017, ARA&A, 55, 303
Kaaret, P., Simet, M. G., & Lang, C. C. 2006, ApJ, 646, 174
Kajava, J. J. E., & Poutanen, J. 2008, in AIP Conf Proc. 1054, Cool Discs, Hot Flows: The Varying Faces of Accreting Compact Objects, ed. M. Axelsson (Melville, NY: AIP), 39
Kennea, J. A., Heinke, C. O., Bahramian, A., et al. 2017, ATel, 10273, 1
Khan, R., Stanek, K. Z., Kochanek, C. S., Thompson, T. A., & Prieto, J. L. 2010, ATel, 2632, 1
Kilgard, R. E., Cowan, J. J., Garcia, M. R., et al. 2005, ApJS, 159, 214
Kim, M., Ho, L. C., Wang, J., et al. 2015, ApJ, 814, 8
King, A., & Lasota, J.-P. 2019, MNRAS, 485, 3588
King, A., Lasota, J.-P., & Middleton, M. 2023, NewAR, 96, 101672
Kluzniak, W., & Lasota, J.-P. 2015, MNRAS, 448, L43
Maccarone, T. J. 2005, MNRAS, 360, L30
McKinney, W. 2010, in Proc. 9th Python in Science Conf., ed. S. van der Walt & J. Millman, 56
McQuinn, K. B. W., Skillman, E. D., Dolphin, A. E., Berg, D., & Kennicutt, R. 2016, ApJ, 826, 21
Merloni, A., Heinz, S., & Di Matteo, T. 2003, MNRAS, 345, 1057
Mezcua, M., Civano, F., Marchesi, S., et al. 2018, MNRAS, 478, 2576
Mezcua, M., Roberts, T. P., Sutton, A. D., & Lobanov, A. P. 2013, MNRAS, 436, 3128
Middleton, M. J., Miller-Jones, J. C. A., Markoff, S., et al. 2013, Natur, 493, 187
Miller-Jones, J. C. A., Strader, J., Heinke, C. O., et al. 2015, MNRAS, 453, 3918
Mitsuda, K., Inoue, H., Koyama, K., et al. 1984, PASJ, 36, 741
Motch, C., Pakull, M. W., Soria, R., Grisé, F., & Pietrzyński, G. 2014, Natur, 514, 198
Nyland, K., Marvil, J., Wrobel, J. M., Young, L. M., & Zauderer, B. A. 2012, ApJ, 753, 103
Paduano, A., Bahramian, A., Miller-Jones, J. C. A., et al. 2024, ApJ, 961, 54
Pakull, M. W., Soria, R., & Motch, C. 2010, Natur, 466, 209
Pannuti, T. G., Schlegel, E. M., & Lacey, C. K. 2006, in IAU Symp. 230, Populations of High Energy Sources in Galaxies, ed. E. J. A. Meurs & G. Fabbiano (Cambridge: Cambridge Univ. Press), 197
Panurach, T., Strader, J., Bahramian, A., et al. 2021, ApJ, 923, 88
Perley, R. A., Chandler, C. J., Butler, B. J., & Wrobel, J. M. 2011, ApJL, 739, L1
Reig, P., Fabregat, J., & Alfonso-Garzón, J. 2020, A&A, 640, A35
Reines, A. E., Condon, J. J., Darling, J., & Greene, J. E. 2020, ApJ, 888, 36
Reines, A. E., & Deller, A. T. 2012, ApJL, 750, L24
Robba, A., Pinto, C., Walton, D. J., et al. 2021, A&A, 652, A118
Rodríguez Castillo, G. A., Israel, G. L., Belfiore, A., et al. 2020, ApJ, 895, 60
Sathyaprakash, R., Roberts, T. P., Walton, D. J., et al. 2019, MNRAS, 488, L35
Shen, P.-X., & Gu, W.-M. 2020, MNRAS, 495, 2408
Shishkovsky, L., Strader, J., Chomiuk, L., et al. 2018, ApJ, 855, 55
Soria, R., Pakull, M. W., Broderick, J. W., Corbel, S., & Motch, C. 2010, MNRAS, 409, 541
Strader, J., Chomiuk, L., Maccarone, T. J., Miller-Jones, J. C. A., & Seth, A. C. 2012, Natur, 490, 71
Strüder, L., Briel, U., Dennerl, K., et al. 2001, A&A, 365, L18
Sutton, A. D., Roberts, T. P., & Middleton, M. J. 2013, MNRAS, 435, 1758
Townsend, L. J., & Charles, P. A. 2020, MNRAS, 495, 139
Tsygankov, S. S., Mushtukov, A. A., Suleimanov, V. F., & Poutanen, J. 2016, MNRAS, 457, 1101
Tudor, V., Miller-Jones, J. C. A., Strader, J., et al. 2022, MNRAS, 513, 3818
Urquhart, R., & Soria, R. 2016, MNRAS, 456, 1859
Urquhart, R., Soria, R., Pakull, M. W., et al. 2019, MNRAS, 482, 2389
van den Eijnden, J., Degenaar, N., Russell, T. D., et al. 2018, Natur, 562, 233
Vasilopoulos, G., Lander, S. K., Koliopanos, F., & Bailyn, C. D. 2020, MNRAS, 491, 4949
Verner, D. A., Ferland, G. J., Korista, K. T., & Yakovlev, D. G. 1996, ApJ, 465, 487
Walton, D. J., Fürst, F., Heida, M., et al. 2018, ApJ, 856, 128
Walton, D. J., Mackenzie, A. D. A., Gully, H., et al. 2022, MNRAS, 509, 1587
Webb, N., Cseh, D., Lenc, E., et al. 2012, Sci, 337, 554
Weisskopf, M. C., Tananbaum, H. D., Van Speybroeck, L. P., & O'Dell, S. L. 2000, Proc. SPIE, 4012, 2
Wilms, J., Allen, A., & McCray, R. 2000, ApJ, 542, 914
Wilson, W. E., Ferris, R. H., Axtens, P., et al. 2011, MNRAS, 416, 832
Wilson-Hodge, C. A., Malacaria, C., Jenke, P. A., et al. 2018, ApJ, 863, 9
Yang, G., Brandt, W. N., Luo, B., et al. 2016, ApJ, 831, 145
Zampieri, L., Mucciarelli, P., Falomo, R., et al. 2004, ApJ, 603, 523
Zhang, Y., Ge, M., Song, L., et al. 2019, ApJ, 879, 61
Zhao, Y., Heinke, C. O., Tudor, V., et al. 2020, MNRAS, 493, 6033